A NOVEL TECHNIQUE TO MONITOR CARBURIZING PROCESSES

Philippe JACQUET[1*], Daniel R. ROUSSE[2]
Gilles BERNARD, Michel LAMBERTIN[1]

[1] LABOMAP, Ecole Nationale Supérieure d'Arts et Métiers, 71 250 Cluny, France
Tel : 33 03 85 59 53 28 ; Fax : 33 03 85 59 53 70, jacquet@cluny.ensam.fr

[2] Département de génie mécanique, Université Laval, Sainte-Foy (Québec), Canada G1K 7P4
Tel : 001 418 656 2131 (3345) ; Fax : 001 418 656 7415, Daniel.Rousse@gmc.ulaval.ca

[*] *Author to whom further correspondence should be addressed.*

ABSTRACT

This paper presents the principle and testing of a novel technique developed for carburizing processes monitoring. The technique relies upon an experimental device made of a thin iron foil with a carburizing atmosphere on one side and a decarburizing atmosphere on the other. The principle of carburizing control is based on the fact that when steady state of carbon diffusion is reached across the thin iron foil, the measured mass flux of carbon on the decarburizing side is related to the inflow of carbon into the parts during the carburizing treatment. Hence, as a probe could be inserted directly into a given furnace, it would provide an *in-situ* control facility. The proposed device could than be used for controlling atmospheric or low-pressure (vacuum) carburizing treatments. The results presented here are limited to atmospheric conditions. Nevertheless, they gave the incentive to the researchers to pursue the development of the device to allow for measurements in a low-pressure furnace and to refine the experimental bench to quantify thoroughly the phenomena involved within the foil.

Key words : **carburizing, decarburizing, diffusion, regulation, control, iron foil.**

NOMENCLATURE

C	Carbon concentration, %
D	Mass diffusion coefficient, cm^2/s
E	Potential, V
I	Intensity, A
J	Conversion factor, 4,19 J/Cal
K	Mass transfer coefficient, cm/s
G	Cell factor
$\dot{m}$	Mass flow rate, mg/h
Q	Activation energy, J/mol
R	Constant, 8.314 J/mol K
R_o	Electric resistance at 0^oC, Ω
t	Time, s, min, h
T	Temperature, K

Greek symbols

α	Temperature correction coefficient
χ	Mole fraction of the specie in the gas
λ_s	Thermal conductivity of the specie, W/m K
λ_G	Thermal conductivity of the gas, W/m K
Δe	Signal of the catharometer, V

Indices and superscripts

0	Reference condition
A	Related to the gas activation energy
C	Carburizing
D	Related to the solid activation energy, diffusion
D	Decarburizing
I	Gas-solid interface
P	Carbon potential
S	Saturation
T	Transition in the chamber

1. INTRODUCTION

It is only since the last two decades that several regulation processes have been available for the regulation of atmospheric carburizing treatments. Many of these rely on devices that monitor the carbon potential (concentration) at atmospheric pressure in the furnaces [1,2]. If any problem occurs, such as a temperature or a pressure drop, the device sends a signal to the regulation program in order to change the length of the cycle or the composition of the atmosphere [3-5]. The use of such regulation systems allows for more homogeneous carbide layers and overall control of the process. Most techniques, such as thermogravimetry, microhardness measurements, electrical resistivity measurements, LEED, are either expensive or not suitable for industrial application or both [6-7].

Moreover, to the best knowledge of the authors, no such regulation process has been made available in the context of low pressure carburizing treatments. This is usually due to the absence of thermodynamic equilibrium [6-7]. As a result, the low pressure carburizing processes is solely modeled by computer [8-12]. Hence, although low pressure carburizing can be more efficient than atmospheric carburizing, the lack of appropriate regulation devices seems to deem its development.

In this context, this paper presents a simple and affordable principle to bridge the gap between this need for regulation in low-pressure atmospheres and the increased performance of carburizing in such conditions.

This paper first introduces the physics of carburizing and the mathematical model which describes carbon diffusion. Then, it presents the proposed regulation device along with several details on the experimental apparatus. The following section focuses on experimental results while the last section summarizes the main conclusions and formulates a few recommendations.

2. CARBURIZING PROCESS

2.1 Physics of carburizing

The physics of carbon diffusion as applied to the proposed device is schematically depicted in Figure 1.

In this figure, the left side of a thin iron foil is exposed to a carburizing furnace atmosphere while the right side of this thin foil is exposed to a controlled decarburizing environment. In such conditions, carbon diffusion occurs across the foil. Figure 1 indicates that propane, C_3H_8, has been used with the proposed experimental apparatus. The principle of monitoring is based on the fact that when steady state is reached in the iron foil, the measured mass flux of carbon on the right side is related to the inflow of carbon into the workload during the carburizing treatment. Hence, as a probe can be inserted directly into the furnace, it provides an *in-situ* monitoring facility.

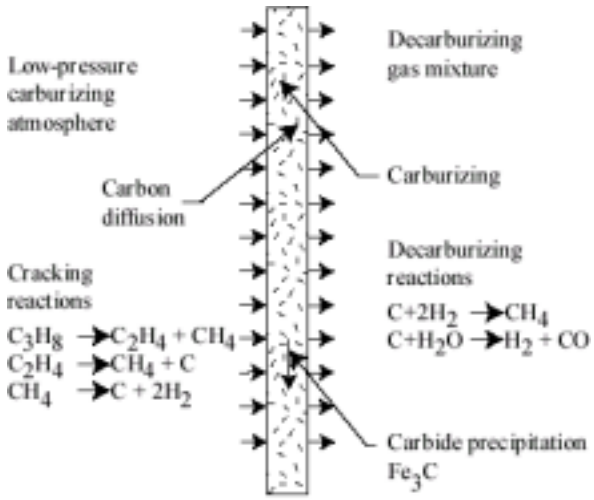

Figure 1: Schematic of carbon diffusion and decarburizing.

Figure 1 also schematically indicates that when the saturation concentration of carbon, C_s, is reached within the foil, precipitation of carbides (Fe_3C) will occur. On the other hand, if the foil is not quenched after the treatment, when the foil carbon concentration decreases below C_s, the carbides will be dissolved within the foil and will diffuse through it.

2.2 Mathematical description of carbon diffusion

The basis for modeling single phase carburizing is the following mass balance equation which states that the total carbon in a differential volume changes in time according to the divergence of the carbon flux plus a volumetric source term of carbon that accounts for carbide precipitation or dissolution:

$$\frac{\partial C(x,t)}{\partial t} = \frac{\partial}{\partial x}\left(D(x,t)\frac{\partial C(x,t)}{\partial x}\right) + S_C(x,t);$$

for $0 \le x \le L;\ t>0$ (1)

in which x is the distance from the carburizing surface, L is the foil thickness, C is the carbon concentration, D is the mass diffusion coefficient, and S_C is the volumetric source of carbon (it is negative in the case of carbides precipitation and positive when carbides are dissolved in the matrix). The boundary and initial conditions are:

$$K_C(t)(C_P - C(x,t)) = -D(x,t)\frac{\partial C(x,t)}{\partial x};$$

for $x=0;\quad t>0$ (2)

$$K_D(t)(C(x,t) - C_G) = -D(x,t)\frac{\partial C(x,t)}{\partial x};$$

for $x=L;\quad t>0$ (3)

$C(x,0) = C_i$; for $0 \le x \le L;\quad t=0$ (4)

where K_C is the mass transfer coefficient on the carburizing side, K_D is the mass transfer coefficient on the decarburizing side, C_P is the carbon potential of the carburizing atmosphere, C_G is the carbon potential of the decarburizing gas, C_G =0, and C_i is the initial concentration of carbon in the material. C_i could be a function of x but for this application the initial carbon concentration is uniform throughout the foil, C_i.=0.

The expressions for D and K have been correlated by several authors for different steels. Ghiglione [13] proposes a review that involves 13 different expressions for D and 9 for K. Here, the following forms are assumed [7]:

$$D(t) = D_0(C)\exp\left(-\frac{Q_d}{RT}\right) \quad (5)$$

$$K_D(t) = K_{D,0}\exp\left(-\frac{Q_a}{RT}\right) \quad (6)$$

in which Q_d is the activation energy of carbon diffusion in austenite, Q_a is the activation energy of the carburizing atmosphere, R=8.314 J/mol K, and T is the temperature in Kelvin.

3. EXPERIMENTAL APPARATUS

To validate the proposed technique, a laboratory experimental apparatus was designed and built. It is schematically illustrated in Figure 2.

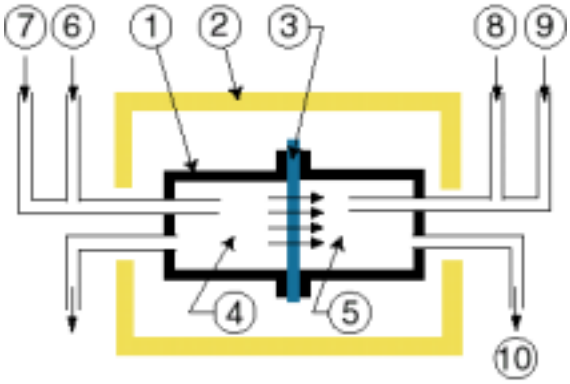

Figure 2: Experimental set-up used to test the concept of the sensor at atmospheric pressure.

In this figure, the experimental cell① is located in a thermally controlled environment②. In the center of this cell① a thin iron foil③ is installed creating two chambers④⑤ which reproduce the configuration of Figure 1. In the following experiments, the foil is made of C100 carbon steel (1%C). On the left side④, a mixture of nitrogen and carburizing gas⑦ is introduced, and on the right side⑤, the decarburizing gas (hydrogen⑧ with a small amount of water vapor⑨) is circulated. The outflow of decarburizing gas is analyzed by a catharometer⑩ [7]. An infrared gas analyzer could also be used.

The catharometer, used for the gas analysis, involves a Wheatstone bridge with a reference flow on one side and the decarburizing flow⑩ on the other side. Once carbon atoms emerge from the right surface of the foil③, the decarburizing reactions produce carbon monoxide, CO, and methane, CH_4 in the chamber⑤. These new substances influence the overall conductivity of the gas mixture and induce a potential in the catharometer. Hence, the increase of the catharometer signal indicates that new types of molecules have appeared in the decarburizing outflow⑩ due to the decarburizing reactions. The sensitivity of the catharometer is given by [7]:

$$\Delta e = \chi \cdot \left[\frac{1}{G}\right] \cdot \left[\frac{\alpha R_o E I^2}{4J}\right] \cdot \left[\frac{1}{\lambda_s} - \frac{1}{\lambda_G}\right] \qquad (7)$$

In this study E=12V, I=250mA, and αR_o=48Ω. The thermal conductivity of the specie at 300K (which is a combination of carbon monoxide, CO, and methane, CH_4) is taken as that of methane, λ_s=34,26 W/mK, and the decarburizing gaz conductivity is that of hydrogen, λ_G=186,86 W/mK (here the water content is neglected) [15]. The cell factor has been evaluated with a hydrogen flow and a hydrogen-vapor flow [7] to yield, G=1,4x10^4. Hence, Eq.7 becomes:

$$\Delta e = 1{,}52\chi \qquad (8)$$

which yields the relationship between the signal and the mole fraction of carbon in the decarburizing gas.

Provided that the total mass flow rate of decarburizing gas, $\dot{m}_G$, is known, it is possible to use Eq.8 to obtain the mass flow rate of carbon:

$$\dot{m}_C = \frac{\Delta e\ \dot{m}_G}{(1.52 - \Delta e)} \qquad (9)$$

Then, the mass flow rate of carbon is divided by the surface area of the foil to yield the mass flux of carbon, $\dot{m}_C^{''}$.

4. RESULTS

Experiments were first carried out with the use of the above-mentioned experimental apparatus (section 3) to establish whether or not the principle could indeed be used to control low-pressure carburizing processes. The carburizing treatments were all carried out at a constant foil temperature of 980°C. While the temperature is rising inside the apparatus, more and more extraction of carbon is observed as the signal diminishes. When both the signal and the temperature are stable, the experiments can begin.

4.1 Foil thickness

The first series of test (figure 3) was carried out to determine the appropriate foil thickness of the proposed probe. A thin foil will lag less than a thicker foil as the diffusion is not instantaneous. However, the foil has to be thick enough to ensure acceptable mechanical properties. Steady state conditions may be reached faster with a thin foil than with a thicker foil but the suggested probe has to be robust enough for use in an industrial furnace.

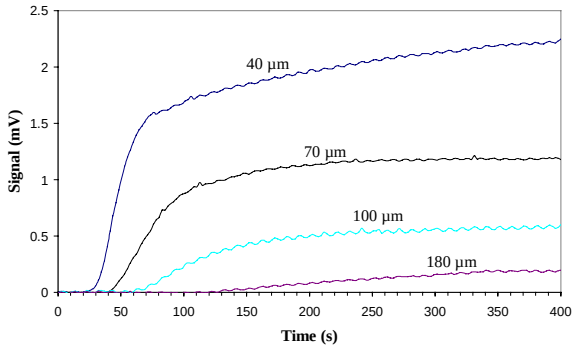

Figure 3: Foil thickness effect on the mass flow rate of carbon and response time.

Six foil thicknesses were tested namely: L = 25 µm, 40 µm, 70 µm, 100 µm, 120 µm, 180 µm. For all tests involved in this section, the decarburizing atmosphere⑤ consisted of pure hydrogen (no water vapor) and injection in the carburizing chamber④ (12s±1s) started after 20s±1s of acquisition time. Physically, soon after the injection the surface concentration reaches C_s on the carburizing side④. This surface concentration is maintained until injection is stopped. In the vicinity of the surface④, carbides begin to precipitate in the matrix and the carbon concentration reaches saturation deeper and deeper in the foil③. Then, when the injection is stopped, the concentration decreases below C_s and carbides begins to dissolve in the matrix③. This explains the two slopes visible (mostly for the thin foils) in figure 3.

Figure 3 immediately reveals that: (1) as the thickness of the foil increases, the response time of the detector augments, and (2) as the thickness increases the maximum value of the signal decreases.

Response time: The measured response time t is the sum of: (1) the diffusion time t_d , (2) the reaction time at the interfaces t_i , (3) the sensitivity time t_s, and (4) the transition time t_t. The time t_d is the quantity of interest while t_t depends of the geometry and the gas flow rate. t_t is a constant evaluated with a perforated foil and measured between the moment the valve is opened and the detection by the catharometer: t_t= 14s for a mass flux of 90 mg/h/cm^2 on both side, for example. t_i is the sorption and desorption reaction time at both gas-solid interfaces, it is assumed negligible compared to t_t. t_s is the time lag between the methane formation on the decarburizing side and the detection by the catharometer. The catharometer posses a sensitivity threshold under which it cannot detect the presence of carbon. However, t_s has been found negligible compared to t_t. Table 1 indicates explicitly the diffusion times obtained with the apparatus.

Table 1: Diffusion time as a function of the foil thickness.

Thickness, L [µm]	Diffusion time, t_d [s]
25	10.8
40	13.9
70	25.0
100	41.1
120	53.2
180	117.0

Amplitude of the signal: A constant signal indicates a constant decarburizing flow rate. Grabke [16] mentions that this decarburizing flow rate is not a function of the carbon content of the steel. This leads to the conclusion that the flow rate is limited by diffusion and hence by the thickness of the foil. Figure 3 clearly indicates this trend although quasi steady state is reached. Steady state can not be obtained with the proposed settings as the carburizing is stopped after 12s±1s. Hence, the concentration of carbon on the left

surface of the foil (figure 1) will not be constant in time after injection is over. Table 2 shows the relation between the mass flux of carbon (converted signal of the catharometer) and the foil thickness.

Table 2: Mass flow rate of carbon as a function of the foil thickness.

Thickness, L [µm]	Mass flux, $\dot{m}_C^{"}$ [mg/h/cm^2]
25	1.06E-01
40	8.46E-02
70	4.23E-02
100	1.90E-02
120	1.41E-02
180	7.75E-03

The table indicates that the mass flux of carbon is approximately inversely proportional to the foil thickness although steady state is not maintained. Here, the mass fluxes are low as the mass flux of decarburizing gas was low (53,50 mg/h/cm^2) and the dew point very low (dry hydrogen has been used, dew point = -40°C).

After several tests, 70 µm was found to be the optimal thickness as it is tough enough to ensure reliability and appropriate mechanical properties: thicker foils are not responding fast enough to ensure an adequate control. The following results are all presented for 70 µm thick foils.

4.2 Carburizing mixture concentration

The optimal carburizing gas concentration to yield the maximum mass flow rate of carbon through the foil was considered next. Experiments proceeded by reducing the concentration of carburizing gas from 18% to 0,4% to detect the threshold indicating this optimal concentration. In this series of test, the foil was first carburized with a mixture of nitrogen and propane during 23s±1s for each experience. A very high mass flow rate of carburizing gas was used to yield a high mass transfer coefficient, K_C. Figure 4 indicates that the valve was opened 220s±1s after acquisition started.

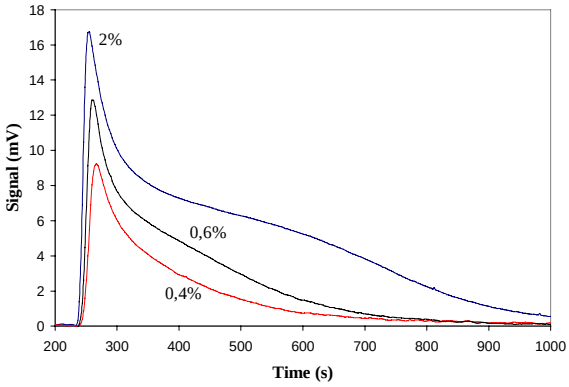

Figure 4: Carburizing gas concentration effect on the mass flow rate of carbon with a short carburizing period.

Typically, concentrations of propane above 2,0% yielded no different maximum mass flow rates of carbon (all curves are superposed): for high concentrations, the responses of the catharometer were nearly identical. With too high a concentration, the mixture is overcarburizing and the excess carbon precipitates as carbides in the matrix; with too low concentration, the carburizing rate is reduced. For the threshold concentration (2% in this case), the gas concentration in the left enclosure is just high enough to yield a surface concentration of carbon nearly equal to C_s. This indicates that a rich mixture is not required to ensure the maximum mass flow and that, at least in principle, the proposed device could be used to calibrate the appropriate gas concentration (carbon potential of the atmosphere). Figure 4 shows sample results for concentrations below the threshold. In this case, absorption of carbon at the steel's surface (the carbon potential, C_P) becomes the limiting step; the mass transfer coefficient, K_C, is not the limiting parameter here as the slope of the curves are all similar.

In a furnace, once the optimum concentration of carburizing gas (the carbon potential, C_P) has been determined, it is possible to increase the carburizing period until steady-state is achieved. In this case, the absorption rate of carbon at the steel's surface and the

diffusion rate are approximately equal. It would also be possible to increase the mass flow rates of carburizing species ⑦ to increase that the mass transfer coefficient, K_C. However, in a furnace, as the ratio of the chamber volume④ to the flow rate is much higher than that of the apparatus, K_C will play a preponderant role: the slopes will not be so steep.

Figure 4 also shows that carbides may precipitate although the maximum mass flow rate may not be obtained. The physics of diffusion without source term (eq.1) should lead to an exponential decrease of the mass flux after carburizing is over. However, the curve for a concentration of 0,6% clearly indicates that carbide precipitated during the carburizing period at least in the vicinity of the surface. Indeed, the curve shows that the decrease in the mass flux is not exponential and that carbides are dissolved in the matrix as the concentration falls below C_s at the surface.

Another series of test was carried out with a longer carburizing period (105s±1s). The results are reported in Figure 5. Here, the graph focuses on the range 250s to 400s, only.

Figure 5 indicates that for each concentration the maximum mass flow rate is obtained within a few seconds after the injection of the carburizing gas. Then, carbides are precipitating and thus the diffusion coefficient diminishes and this leads to a decrease of the mass flow rate of carbon. The differences between the curves after 290s could be due to the fact that for the higher concentrations in the carburizing gas the carbon gradient in the foil is higher for a similar diffusion coefficient. However, the uncertainties on the measurement of the mass flow rate of carbon and on the exact content of water in the decarburizing gas do not permit an absolute conclusion.

The interest in Figure 5 is the shape of the curves after the carburizing period is over (t = 360s). A second peak is obtained for each curve. This tends to confirm that as the content of carbon in the foil falls below C_s when carburizing stops, the carbides are dissolved and the diffusion coefficient augments. X-ray analyses showed for SCL415 that 60s after the carburizing step, carbides (Fe_3C) are completely dissolved [19].

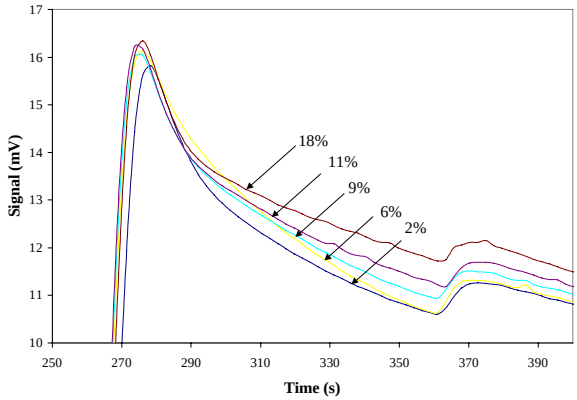

Figure 5: Carburizing gas concentration effect on the mass flow rate of carbon with a long carburizing period.

4.3 Carburizing period and mixture

The third parameter to be studied was the length of the period of the «boost-diffusion» carburizing step for two different carburizing mixtures. As shown in Figure 6, the maximum value of the mass flow rate of carbon is similar for all carburizing periods from 10s±1s to 230s±1s provided that the same decarburizing rate was used (same mass flux and water content) and that the carburizing gas concentration was above 2% (the surface concentration of carbon equals C_s). For this test case, a mixture of hydrogen and propane was used④.

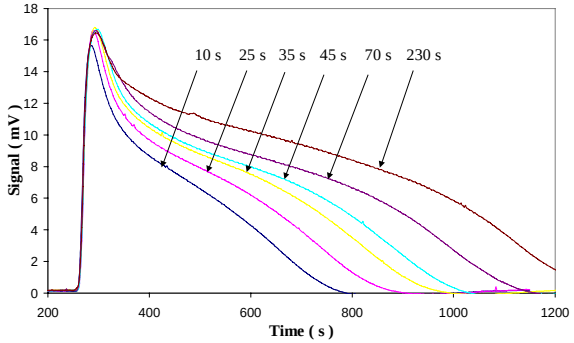

Figure 6: Carburizing period effect on the mass flow rate of carbon (hydrogen/propane mixture).

For this series of experiments, the peak height is determined by the decarburizing rate and is proportional to this rate. This rate is in turn a function of the mass flow rate of the hydrogen-water vapor mixture⑤ as well as its composition. Here, the second peak due to the sudden increase of the diffusion coefficient is merely detectable as hydrogen was used instead of nitrogen to carburize. Initially, the signal recorded by the catharometer is constant indicating that no carbon has crossed the foil. Then, the signal steeply increases a few seconds after the injection of the carburizing gas: the surface concentration of carbon reached C_s almost instantaneously. The response is expected to be different in a furnace or with a lower water content of the decarburizing gas as shown in Table 1 for L= 70 µm.

In Figure 6, injection of carburizing mixture starts at t = 220s±1s. Here again, the inertia of the whole apparatus has been found by subtracting the time constant (t_t + t_s + t_i) of the fluid flowing through the system to the total time recorded.

The surface under each curve in Figure 6 corresponds to the amount of carbon that has diffused through the foil. This quantity divided by the carburizing time and by the surface area of the foil yields the average mass flux of carbon.

The shape of the curves in Figure 6 also indicates that when the carburizing period increases, there is an increasing amount of carbide that precipitates within the foil: the area under each curve is different and the maximum flux is similar. Also, it is shown again that the presence of carbide in the steel diminishes its ability to diffuse carbon: D decreases. This is indicated by the slopes of the curves after the peaks: the steeper the slope, the lower the amount of carbide provided that the carburizing period is shorter.

Figure 6 also indicates that the time required to reach the initial level (no flow rate) after carburizing is stopped increases with increasing periods. This indicates that when the carburizing period is over, the carbides start to be dissolved in the steel. When, the process is over, the carbon concentration in the foil is back to C_i. The successive carbide precipitation and dissolution in the iron matrix (leading to a modification of the diffusion coefficient) has also been reported by Sugiyama, Ishikawa et Iwata [19].

In Figure 7, results are shown for a mixture of nitrogen and propane (0,5%), for the range 200s to 500s, only.

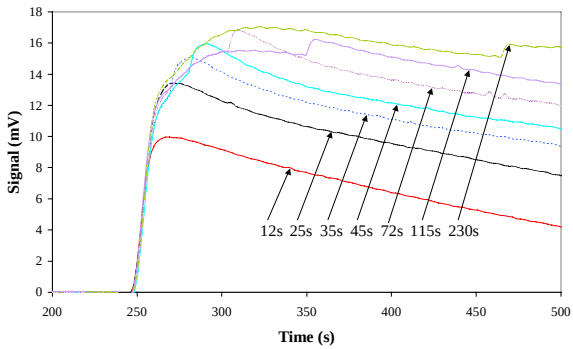

Figure 7: Carburizing period effect on the mass flow rate of carbon (nitrogen/propane mixture).

Here, the period influences the maximum mass flow rate of carbon as the concentration is below the threshold concentration (2%) and the end of each carburizing period is clearly identified by the second peak obtained when nitrogen is used instead of hydrogen in the carburizing mixture.

4.4 Dew point of the decarburizing mixture

The decarburizing gas is a mixture of hydrogen⑧ and water vapor⑨ with a composition that should be calibrated to ensure a maximum decarburizing potential without the risk of oxidation. In fact, two alternatives could be considered to increase decarburizing rates: an increase of the mass flow rate and/or an injection of water vapor in the hydrogen. Bracho-Troconis [18] investigated the effect of the mass flow rate of decarburizing gas on the decarburizing rates for a given water content (dew point at –20°C). Here, the effects of the variation of the dew point of the mixture are investigated. An important increase of the mass flow rate of hydrogen would lead to a lower sensitivity of the catharometer which is an undesirable effect.

Figure 8 reports the effects of the dew point of the mixture on the mass flux of carbon (signal of the

catharometer) for a constant decarburizing gas flux⑧⑨ of 157.36 mg/h/cm^2.

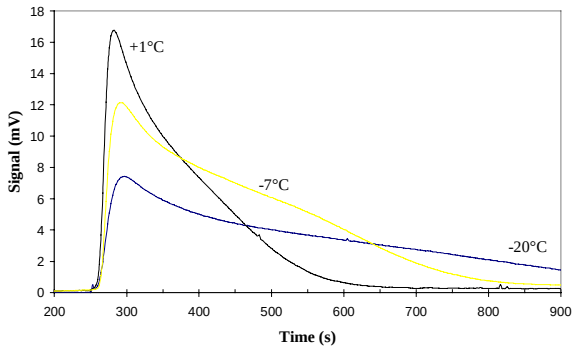

Figure 8: Decarburizing gas composition effect on the mass flow rate of carbon.

Injection periods of 12s±1s were considered for each experiment. Figure 8 shows two things: (1) the maximum mass flux increases with the water content as a second decarburizing reaction occurs at the interface: $C+H_2O \rightarrow CO+H_2$; and (2) the rate at which carbon is removed after injection is stopped is also more important with increasing water content (the signal gets back to zero faster when the water content is important). In fact, the second reaction ($C+H_2O \rightarrow CO+H_2$) becomes preponderant over the combination of hydrogen and carbon into methane. Indeed, Grabke [17] showed that for dew points above 7°C, the reaction rate due to hydrogen is negligible compared to that due to water vapor. However, the dew point should not be too high to avoid the risk of oxidation. In the following tests, a mixture with a dew point of about 0°C (corresponding to a water vapor partial pressure of 613 Pa) has been used [17].

For the results presented in figure 8, the area under each curve is identical (within experimental uncertainty) as the total amount of carbon introduced by the carburizing process is similar in each case. The injection period is the same for the three cases.

4.5 Average mass flux of carbon

To complete the results, the average mass flux for the tested carburizing periods (figure 6) with overcarburizing atmosphere is reported in Table 3.

Table 3: Decarburizing time and average mass flux of carbon for several carburizing periods.

Carburizing period [s]	Decarburizing time [min]	Average mass flux [mg/h/cm^2]
10	9.2	30
25	10.8	15
35	12.3	13
45	13.0	11
70	15.1	8,6
230	17.5	3,3

The table indicates that the mass flux is very high at the beginning of the carburizing sequence, but decrease very rapidly as carbon atoms saturate the steel and form carbides that diminish *D*. The results reported in table 3, compared to those in table 2, also clearly show the effects of the water content in the decarburizing mixture.

In summary, this test indicates that when the atmosphere is overcarburizing, the precipitation of carbide influences the mass diffusion and that carburizing steps, along with corresponding diffusion steps, are needed to obtain a better diffusion. Hence, the carburizing atmosphere should be controlled to ensure that the surface concentration of carbon remains just below C_s. This would allow for continuous carburizing at a maximum rate without the risk of sooting. Here again, results suggest that the proposed device could be used to monitor the process.

4.6 Long cycles

Figure 9 proposes the last example of some of the results obtained with the experimental cell① for long carburizing periods (40 min). Here, the carburizing gas was a mixture of nitrogen and propane to investigate the possible presence of the second peak that occurs when the carburizing is stopped.

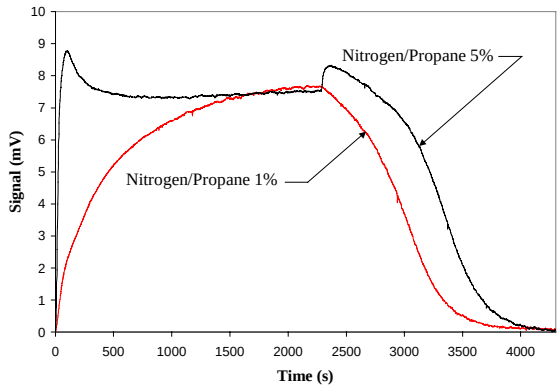

Figure 9: Carburizing period effect on the mass flow rate of carbon (nitrogen/propane mixture).

Two curves are shown on figure 9: the first for a concentration of 5% and the other for 1%.

1% concentration: When the gas concentration is below the threshold of 2%, the mass flow rate of carbon detected by the catharometer slowly increases until steady state is obtained. This contrast with results shown in figure 4 for which a high mass flow rate of gas④ allowed for a quick response. While the concentration of carbon slowly increases in the foil, the diffusion rate is high enough to balance the carburizing potential effect of the atmosphere on the surface absorption. The saturation concentration is reached at the surface④ as the asymptote is close to the other curve (the discrepancies are due the slight variation of the dew point of the decarburizing atmosphere). Here, the kinetics of diffusion and precipitation/dissolution of carbides are in a local equilibrium state throughout the foil.

5% concentration: When the gas concentration is equal to or above the threshold of 2%, the mass flow rate of carbon detected by the catharometer steeply increases to reach a maximum value. Carbides precipitate and the diffusion coefficient decreases slowly as the kinetics of carbide precipitation is slower than that of carbon diffusion. A permanent regime is obtained, as long as the carburizing atmosphere is maintained, as the maximum concentration of carbide is obtained on the surface. Then, as previously observed, when the carburizing period is over, carbides are dissolved.

The curves are interestingly different after injection (t= 2400s). The foil carburized with the overcarburizing atmosphere (5%) shows an increase of the mass flow rate of carbon and then a decline similar to that of the other result presented here. The foil carburized with a poor atmosphere (1%) does not behave as the other one: the mass flux does not increases. This suggests that more carbides precipitated with the rich atmosphere and that this extra amount of carbides did not influence the diffusion coefficients as both steady states occur at the same flux (about 7,4 mV, figure 9). Moreover, this formation of carbides could be due to an oversaturation of the foil in a non equilibrium state at the beginning of the cycle. Then, the first peak (5% curve) could be due to an instantaneous concentration of carbon superior to C_s before precipitation occurs combined with a diffusion coefficient unaffected by the carbides. This would then explain the second peak, indicating more carbides when the carbon potential is higher. As mentioned earlier, for the second curve (1%), the kinetics of diffusion would be of the same order of magnitude than that of precipitation and thus the reactions would be in equilibrium throughout the process.

However, it has not been possible to verify the above mentioned assumption thoroughly with the apparatus. Further experiments and analyses of the foil after carburizing (and quenching) would be required to go one step beyond Sugiyama, Ishikawa et Iwata [19] in the investigation of the kinetics of precipitation/dissolution of carbides.

5. CONCLUSION

5.1 Contributions

This paper presented the principle of a novel regulation device that could be used in atmospheric or low-pressure (vacuum) conditions. The sample results indicate that the device could be used to monitor and

control the carburizing process of steel in furnaces. It could be used to:

- study the impact of the carburizing gas mass flow rate and concentration on the mass flow rate of carbon;
- develop carburizing cycles that do not require diffusion steps;
- investigate the effect of the variation of selected parameters;
- provide data for simulation programs based on the solution of transient mass diffusion with convective boundary conditions;
- quantify the rate of carbide precipitation and dissolution within the steel matrix.

5.2 Current work

1. The first project undertaken after this first series of result was concerned with a refinement of the experimental apparatus in order to reduce the experimental uncertainties of the measurements. This will allow to quantify what has been observed with the first set-up and strengthen the conclusion, especially those pertaining to the kinetics of carbide precipitation and dissolution.
2. Another fundamental aspect of the problem should be investigated, that is the kinetics of diffusion vs that of the precipitation of carbides. This would help in providing a better explanation for the two peaks obtained when overcarburizing conditions are imposed.
3. It should also be interesting to apply the proposed principle to the design of a sensor to be used in a real furnace: this is now also being done in a BMI low-pressure carburizing furnace.
4. Moreover, it would be relevant to obtain correlations between the mass flow rate of carbon in the sensor and that in the workload of the furnace as a function of the workload geometry and properties and the furnace configuration. This is the subject of current work by the authors: two main projects are actually underway: (1) experimental measurements in a prototype furnace; and (2) numerical simulation of the process.

6. REFERENCES

[1] Bond, H.W., Dispositif de mesure et de régulation du potentiel carbone: vue d'ensemble et historique. Traitement thermique, n°235, Mars 1990, pp.pp.29-31.

[2] Sobusiak, T., Method of mesuring carbon potential and carbon transfer coefficient. HEAT TREATMENT SHANGAI'83. Proceedings of the Third International Congress on Heat Treatment of Materials, 7 - 11 November 1983, Shangai, Edited by professor T. Bell, pp.1.79-1.85.

[3] Aubry, R., Optimisation de la cémentation gazeuse en four continu par pilotage automatique. Traitement thermique, n°174, Mai 1983, pp.49-63.

[4] Lipinsky, A., and Suryn, W.L., Using programmable control systems in heat treatment processes. HEAT TREATMENT SHANGAI'83. Proceedings of the Third International Congress on Heat Treatment of Materials, 7 - 11 November 1983 Shangai, Edited by professor T. Bell, pp.4.36-4.40.

[5] Edenhofer, B., and W. Lerche, Developments in process technology and procedure of gas carburizing. Härterei - teschnische Mitteilungen,. vol. 49,n°2, pp.88-95,1994.

[6] Jacquet, P., Bernard, G., Jomain, B., Souchard, J.P., and Lambertin, M., Développement d'un capteur de suivi pour la cémentation basse pression des aciers, Traitement Thermique n°312, Novembre 1998.

[7] Jacquet, P., Cémentation basse pression des aciers. Développement d'un capteur de suivi, Thèse ENSAM, Cluny, 1998, 144 p.

[8] Goldstein, J.I., and Moren, A. E., Diffusion modeling of the Carburization Process, Metallurgical transaction A, vol. 9A, November 1978, pp. 1515-1525.

[9] Madsac, M., Queille, P., Kostelitz, M., Prévision des profils de concentration en carbone à partir d'un modèle de cémentation gazeuse, Application à l'optimisation des cycles thermiques. Traitement thermique, n°174, Mai 1983, pp.19-25.

[10] Morral, J.E., Dupen, B.M., and Law, C.C., Application of Commercial Computer Codes to the Modeling Carburizing Kinetics of Alloy Steels. Metallurgical Transactions A, vol. 23A, 1992, pp. 2069-2071.

[11] Pavlossoglou, J., A new optimisation model of boost-diffusion cycle for infinite surface steel plates / cylinder to minimise time for desired carbon profile. HEAT TREATMENT SHANGAI'83. Proceedings of the Third International Congress on Heat Treatment of Materials, 7 - 11 November 1983 Shangai. Edited by professor T. Bell, pp.1.86-1.96.

[12] Stickels, C. A., Analytical Models for the Gas Carburizing Process. Metallurgical Transactions B, vol. 20B, 1989, pp. 535-546.

[13] Ghiglione, D., Modèles mathématiques de cémentation, Traitement thermique, n°195 , pp.31-39, 1985.

[14] Deshayes, J. Germain, P. Jacquot, E. Denisse, G. Dervieux, La cémentation basse pression des aciers. Traitement thermique, n°261 Janvier/ Février 1993, pp.22-30.

[15] Handbook of Chemistry and Physics, 55th Ed., CRC Press, Cleveland, 1975, p.E-2.

[16] Grabke, H.J., Kinetics and mechanisms of gas-metal interactions, Ann. Rev. Mat. Sci., vol.7, 1977, pp.155-178.

[17] Béranger, G., Henry, G., and Sanz, G., Le livre de l'acier – Technique et documentation, Lavoisier, Paris, 1994, p.233.

[18] Bracho-Troconis, C.B., Décarburation d'acier doux; cinétique et mécanismes d'échanges de matière (carbone) à l'interface métal-gaz dans les atmosphères complexes., Thèse UTCompiègne, Septembre 1990, p. 188.

[19] Sugiyama, M., Ishikawa, K., Iwata, H., Using Acetylene for Superior Performance Vacuum Carburizing, Proc. 18th Conf. Heat Treating, 12-15 october 1998, pp.49-56.